Available online at www.sciencedirect.com
SCIENCE DIRECT®
C. R. Chimie 8 (2005) 713–726
COMPTES RENDUS CHIMIE
http://france.elsevier.com/direct/CRAS2C/

Account / Revue

Highly ordered mesoporous CMI-*n* materials and hierarchically structured meso–macroporous compositions

Bao-Lian Su *, Alexandre Léonard, Zhong-Yong Yuan

Laboratoire de chimie des matériaux inorganiques, université de Namur (FUNDP), 61, rue de Bruxelles, B-5000 Namur, Belgium

Received 27 July 2004; accepted after revision 8 October 2004

Available online 17 February 2005

Abstract

The present review outlines the research work realized during last the 10 years in our laboratory in the field of the conception of new nanostructured porous materials, from mesoporous silicas and metal oxides to hierarchical meso–macroporous compounds with various compositions (single and binary metal oxides and aluminosilicates, aluminophosphates and silicoaluminophosphates). An accent was especially made on the evolution in the development of new synthesis strategies for the introduction of a hierarchy in one solid body with and without surfactant molecules. ***To cite this article: B.-L. Su and al, C. R. Chimie 8 (2005).***

Résumé

Cette publication décrit les travaux de recherche réalisés au laboratoire CMI au cours des dix dernières années dans le domaine de la conception de matériaux poreux nanostructurés, depuis les matériaux mésoporeux hautement structurés (silice et oxydes de métaux de transition) jusqu'à des matériaux plus sophistiqués (oxydes de métaux de transition simples et binaires, aluminosilicates, aluminophosphates et silicoaluminophosphates). Un accent tout particulier est mis sur l'évolution dans la recherche de nouvelles stratégies de synthèse pour l'introduction d'une hiérarchie de la porosité dans un corps solide unique, avec ou sans molécule de surfactant. ***Pour citer cet article : B.-L. Su et al, C. R. Chimie 8 (2005).***

Keywords: Mesoporous; Multiporosity; Metal oxides; Silica; Aluminophosphates; Aluminosilicates; Surfactant-templating

Mots clés : Mésoporeux ; Oxydes simples et binaires de métaux de transition ; Silice ; Aluminosilicates ; Aluminophosphates ; Silicoaluminophosphates ; Surfactant

* Corresponding author.
E-mail address: bao-lian.su@fundp.ac.be (B.-L. Su).

1631-0748/$ - see front matter © 2005 Académie des sciences. Published by Elsevier SAS. All rights reserved.
doi:10.1016/j.crci.2004.10.012

1. Introduction

More than 10 years past since the discovery of the so-called M41S mesoporous silica materials, the preparation of periodic mesoporous materials with different compositions has been gaining increasing attention. The surfactant-templating method has been extended to the synthesis of non-silica oxide mesoporous materials [1–8]. And enormous application potential of mesoporous transition metal oxides has been found in the fields of electromagnetics, photoelectronics, catalysis and separation [9]. By using firstly cationic surfactants and then non-ionic polyoxyethylene alkyl ethers (POE), a series of highly ordered mesoporous silicas and metal oxides were conceived in our laboratory [10–24]. The non-ionic POE type surfactants are indeed of considerable interest as they are low-cost, biodegradable and less toxic than the commonly used quaternary ammonium derivatives in MCM-41-type materials synthesis. The main advantage of this kind of surfactant molecules relies not only on the H-bonding type interactions between the surfactant and the inorganic sources allowing an easier removal of the templating molecule to create the open mesoporous framework, but also on the flexible and tuneable hydrophilic groups which offer the control of the pore size and geometry by varying the hydrothermal conditions and by using freezing agents of the polyoxyethylene unit such as transition metal ions [17,18].

The development of modern and environmental friendly industrial processes with the highest efficiency and the lowest energy and brut materials consumption requires the more advanced and sophisticated materials having hierarchical pore structures at different length scales in order to achieve highly organized functions. Mesoporous oxide materials with macroporous structures have shown to be of great interest as potential catalysts and sorbents, partly because the textural mesopores and intrinsic interconnected pore systems of macrostructures should be able to efficiently transport guest species to framework binding sites. FCC catalysts are the concrete example of hierarchical structure in use in industry and involve the formation of a composite principally from a main component, an USY zeolite mixed with a macroporous matrix, usually amorphous silica, alumina or silica/alumina with clay. A pre-cracking of the heavy feedstocks prior to the action of the USY zeolite is carried out in macroporous matrix. The microporous openings of zeolites impede however the diffusion of bulky molecules from vacuum gas–oil and residues. The introduction of mesoporosity in USY zeolite by vapor steaming treatment can facilitate thus the secondary catalytic cracking. Finally, the more oriented cracking and the fine rearrangement of cracked molecules take place in the supercages of USY zeolite. However, this micro–meso–macroporous hierarchy was obtained by artificial mixture of different components containing pre-defined porosities.

The combination of surfactant-templating techniques and colloidal crystal templating methods allows the construction of hierarchically bimodal meso–macroporous silicas [25–29]. Polymeric latex spheres were largely used as templating agent for the macroporosity generation [25,26,30]. However, the design of high surface area materials with multi-scaled porous structure has still remained an experimental challenge. The development of new methods for hierarchical porous materials conception should be thus of great importance.

The present paper describes the evolution from highly ordered mesoporous CMI-n materials to our very recent success in hierarchically structured meso–macroporous single and binary oxides and aluminosilicates, aluminophosphates and silicoaluminophosphates. We just want to shed some light on the conception of sophisticated materials.

2. Hexagonally ordered mesoporous CMI-*n* materials

2.1. Evolution of the structural, textural and morphological features of CMI-1 materials upon the variation of surfactant weight percentage (SWP)

We start this review by the preparation of highly ordered mesoporous CMI-1 molecular sieves by using non-ionic POE type surfactants. This type of surfactant has been largely used for the synthesis of a series of mesoporous silicas and metal oxides [5,31–40]. The particularity of this part of work relies on its soft synthesis conditions (mild acidic conditions, pH 2) [10,11,15–21].

When the SWPs used are superior to 30, i.e. within the domain of the hexagonal liquid crystalline phase in

pure aqueous solution [41–43], the materials obtained exhibit a disordered channel array as shown from low angle XRD and transmission electron microscopic (TEM) observations (Figs. 1 and 2). Nevertheless, the presence of a single reflection line on the XRD pattern proves the homogeneity in the channel sizes as it is representative of the average pore-to-pore separation.

For the lower SWPs (< 30), the low-angle XRD patterns show three well-defined reflection lines which can be indexed on a hexagonal unit cell and thus indicate the hexagonal symmetry in the stacking of the channels. Honeycomb-like pore arrays observed by TEM confirm these observations.

At the SWP equal to 30, the XRD pattern shows surprisingly two intense neighboring reflection lines, which might be suggestive of the coexistence of two phases, the disordered and the ordered one.

The particle morphologies are also significantly affected by the surfactant concentration. Indeed, for the high weight percentages, irregularly-shaped blocks of different sizes are formed, whereas for diluted solutions, the only morphologies are spheres of 1–2 μm by diameter (Fig. 1). The spherical morphologies that go along with the hexagonal stacking of the channels could be used for column packing in chromatography as irregular particles tend to break down [44–47]. Some TEM observations of ordered samples exhibited fingerprint-like channel arrays which could be the result of the section of a sphere where the channels are running concentrically (Fig. 2C).

The textural study shows that all the compounds are mesoporous. The pore size distributions (PSD) show well-defined maxima centered between 3.6 and 4.9 nm (Fig. 1). A more peculiar shape of the isotherm and the PSD has been evidenced for a weight percentage of 30. This has been attributed to the possible coexistence of two types of structures with probably different pore openings [48,49] in the final materials. The specific surface areas of all the final materials are superior to 800 m^2/g.

For the more concentrated micellar solutions, two effects that lead to wormhole-like materials have to be

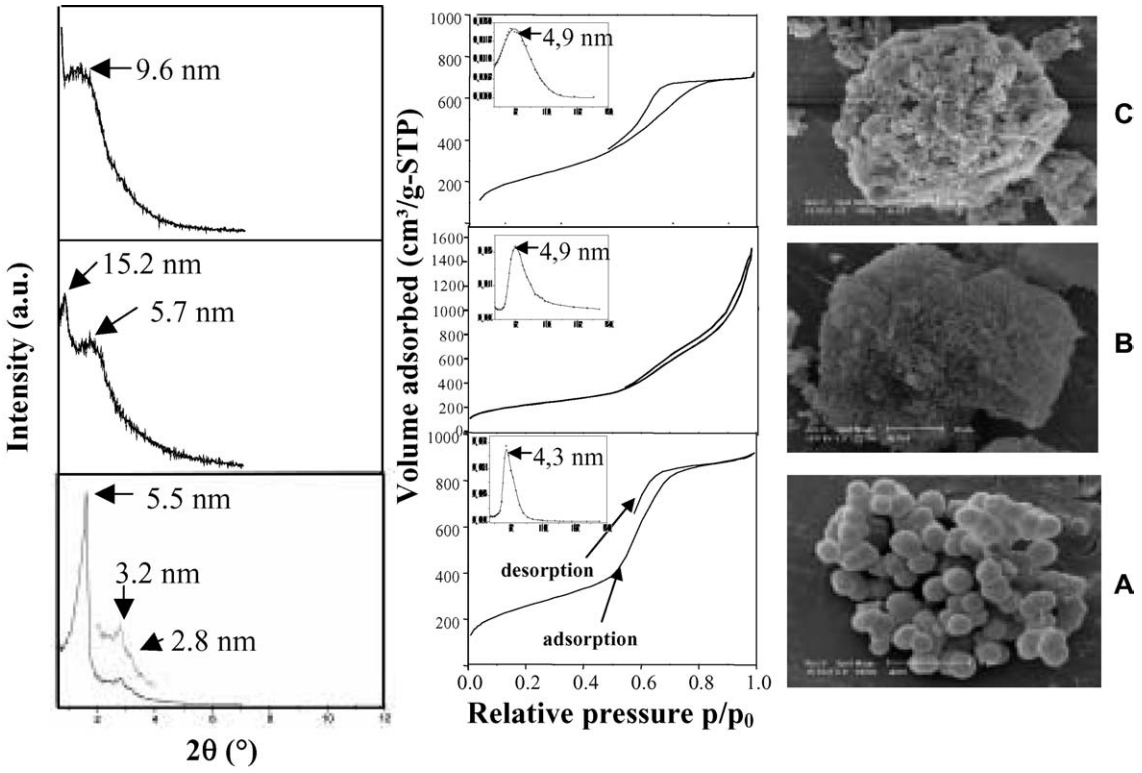

Fig. 1. Low-angle XRD patterns, nitrogen adsorption–desorption isotherms with corresponding PSDs and SEM pictures representing a sample prepared (**A**) at a concentration inferior to 30 wt.%, (**B**) at 30 wt.% and (**C**) for the higher concentrations (>30 wt.%) of template.

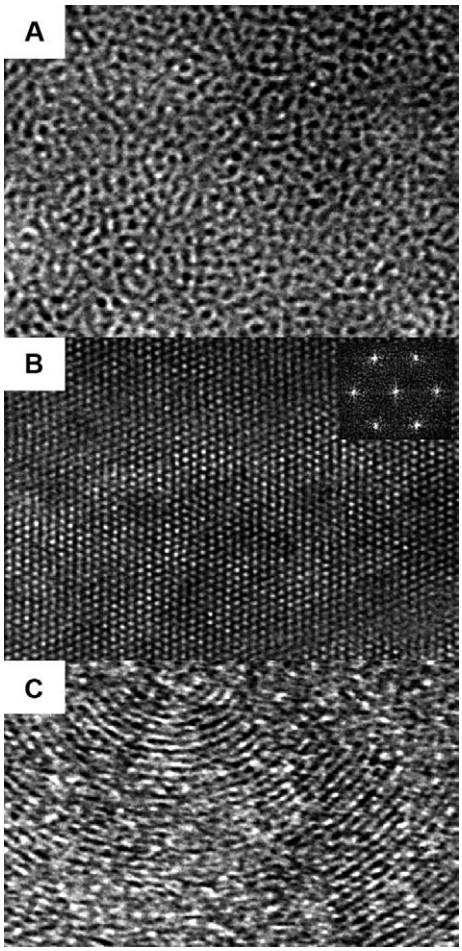

Fig. 2. TEM pictures of (**A**) a disordered wormhole-like structure (> 30 wt.%), (**B**) a regular hexagonal framework and (**C**) a 'fingerprint'-like arrangement of channels (< 30 wt.%).

taken into account. The most important one arises from the silica polymerization. When the hydrolyzed silica species interact with the hydrophilic groups of the surfactant, their polymerization at the organic–inorganic interface will provoke a deformation of the surfactant–silica rods in order to minimize steric and electrostatic energies. This will lead to a loss of the regular stacking of the channels. The second effect concerns the release of methanol during silica hydrolysis and condensation. Indeed, it was reported that this molecule has a liquid crystal breaking effect [31].

On the other hand, the formation of ordered hexagonal structures from the diluted micellar solution (SWP < 30) can be expected by a cooperative mechanism [3,41,42,44].

At 30 wt.%, the ordered and disordered phases are simultaneously detected. There could be a competition between these two formation mechanisms, which explains the dual nature of the materials as observed from the different characterization techniques.

2.2. Evolution of the structural and morphological features of CMI-1 materials upon the variation of the pH value of the synthesis gel

The pH of the synthesis gel is an important factor as it greatly affects the inorganic source hydrolysis and polycondensation. The rates of these processes will in their turn influence the characteristics of the final obtained phases.

The pH value of the starting micellar solutions was varied between 0.5 and 12. Due to the release of silicic acid during hydrolysis of TMOS and the polymerization of resulting siliceous species, the pH value of the gel are quite different from that of the starting micellar solution and significantly decrease. The higher pH value of starting micellar solution is, the more important drop in pH value after addition of silica source is observed. For example, the pH value of the starting solution decreases from 10 to 7.0, 8.5–6.5 and 5.0–4.5 while the pH value of 0.5 and 2 of starting solution remains unchanged. For all of the acidic or neutral synthesis gels, the materials obtained exhibit a highly ordered hexagonal framework evidenced by low angle XRD and TEM. As the nature and charges of the silicic species vary with the pH, the surfactant–silica assembly will still be formed via a cooperative mechanism but, depending on pH, involving positively or negatively charged counterions. CMI-1 materials with hexagonal stacking of their channels can successfully be prepared thus under acidic, neutral or basic media. Changes however occur regarding the morphology. Exotic shapes are observed if the starting micellar solution has a pH value below 2. As the pH increased, these shapes evolve towards an assembly of very small submicrometric spheres with high interstitial porosity. This evolution has been related to the sharp increase in the nucleation and polycondensation rate of the silica source with pH value [48]. Interestingly, for the very acidic synthesis gels, gyroids, toroids, ropes, ... were observed but no regular stacking of the mesoporous channels could be evidenced, suggesting no direct relationship between the structure and the outer morphology of the materials.

2.3. Control of the morphology of ordered CMI-1 mesoporous materials by adjusting the surfactant/silica molar ratio

The texture as well as the morphology of ordered mesoporous molecular sieves is an important factor that has to be controlled for industrial applications [49–57]. The aim of this part is to present an avenue worth exploring in control of the morphologies by varying the relative amount of the inorganic source with respect to the surfactant.

At 80 and 40 °C for a wide range of surfactant/silica molar ratios (*R*) (0.25–3.50), highly-ordered hexagonal structures were obtained [11] for the high amounts of added silica. The regularity however decreases with raising *R*-value where the system could not be as rigidified due to the lower inorganic content, which could lead to a gliding of the channels during hydrothermal treatment, leading to more wormhole-like phases as just mentioned in above section. A more peculiar behavior was however observed at 60 °C as the structures were less ordered and the pore sizes decreased.

The most outstanding influence of varying *R* concerns the morphology (Fig. 3). For all the investigated hydrothermal treatment conditions, for the very high amounts of added silica source, gyroidal, toroidal and rope-like shapes have been obtained. These could arise from local rigidification effects that lead to specific local deposition of the silica species, affording thus directional growing of the particles [53,58]. For higher *R* values, the morphologies evolve towards spheres at 60 and 80 °C and to highly porous irregularly-shaped blocks at 40 °C.

2.4. Synthesis of highly ordered CMI-2 and -4 materials by the complexation of transition metallic cations by the oxyethylene heads of the surfactant

Another way to produce highly ordered mesoporous channel arrays by using non-ionic POE surfactants was proposed a few years ago by Zhang et al. [59]. These authors induced an electrostatic control of the surfactant–silica assembly by complexing transition metallic cations by the hydrophilic oxyethylene heads of the non-ionic POE surfactant.

Ordered materials CMI-2 [10,17,18] with a hexagonal stacking of their channels have successfully been prepared by adding Co^{2+} cations to 50 wt.% $C_{16}(EO)_{10}$ micellar solutions. As explained above, the same sur-

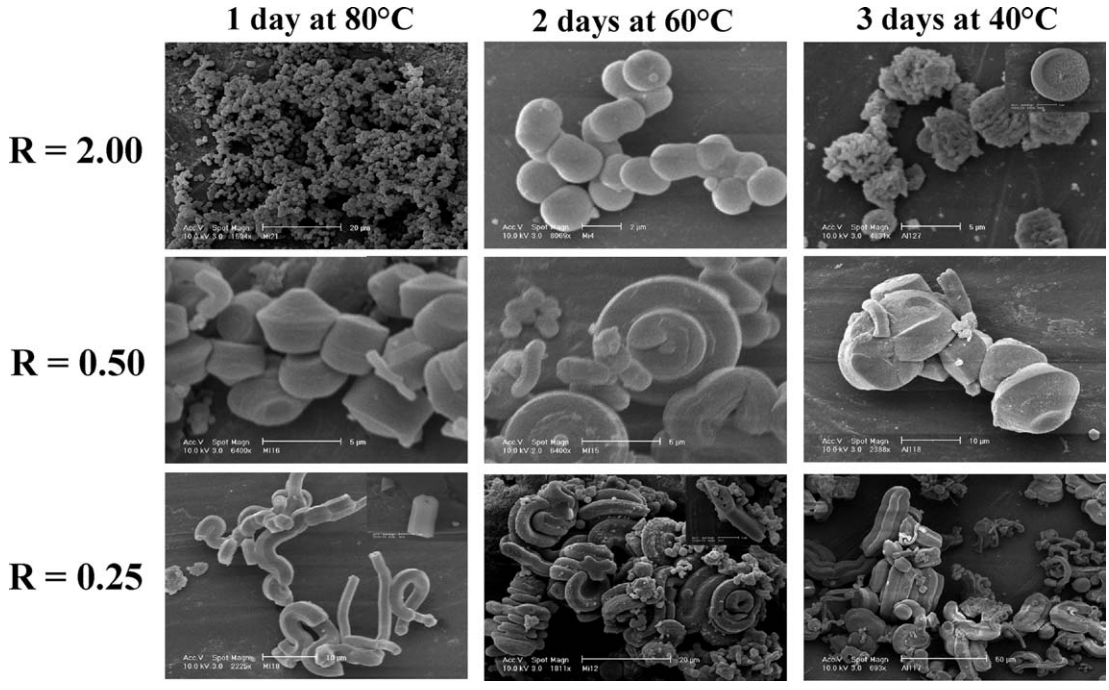

Fig. 3. SEM pictures of samples prepared at 80, 60 and 40 °C and with surfactant/silica molar ratios of 0.25, 0.50 and 2.00.

factant concentration usually leads to wormhole-like frameworks in spite of the existence of a hexagonal liquid crystal phase prior to the addition of the inorganic source. The hexagonal ordering can be evidenced by the TEM pictures. The SWP has additionally been varied using $C_{18}(EO)_{10}$ and cobalt cations. From the low angle XRD patterns (Fig. 4), highly ordered hexagonal mesoporous structures can be synthesized for SWP inferior to 40. This shows that when using the complexation of cations by the heads of the surfactant, the domain of SWP where ordered materials (CMI-4 [10,17,18]) can be obtained is enlarged. The presence of cobalt ions probably induces some changes in the packing parameter of the surfactant, as its value is related to the hydrophobic tail length, the molecule volume and to the surface of the PEO head, which is modified upon complexation.

When comparing the structural features of materials prepared at low SWP (e.g., 10 or 20) with and without cations, it appears that the hexagonal stacking of the channels is even improved in the presence of cobalt ions.

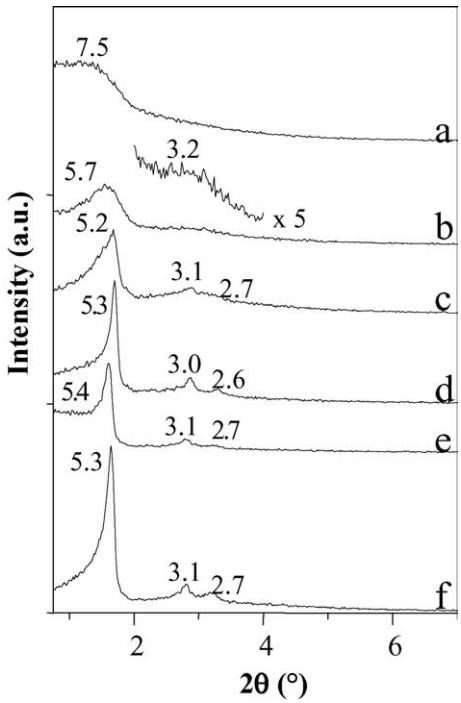

Fig. 4. XRD patterns of compounds prepared with solutions containing 0.705 M Co^{2+} as a function of $C_{18}(EO)_{10}$ weight percentage: a: 50, b: 40, c: 30, d: 20, e: 10 and f: 5 (d-spacings in nm).

Some attempts have also been made with nickel ions, but ordered materials could only be obtained for the very low SWPs.

3. Nanostructured mesoporous metal oxides

Due to the large field of applications ranging from catalysis to ceramics, among the non-silica mesoporous oxides, zirconia is of particular interest. ZrO_2 can catalyze or is a catalyst support for various reactions such as the catalytic reduction of aldehydes and ketones with 2-propanol [60] or the hydrogenation of aromatic carboxylic acids [61]. Using cationic [62], amphoteric [63], anionic [64], or neutral [65] templates and, depending on the synthesis pathway, zirconyl chloride or zirconium propoxide as zirconium precursors, hexagonal, cubic or disordered mesoporous zirconia were successfully obtained. A systematic kinetic study of mesoporous zirconia formation has been performed in our laboratory [13] in order to optimize the synthesis conditions by using cetylmethylammonium bromide as surfactant and zirconyl chloride as inorganic source.

The broad reflection line in the range of $25° < 2\theta < 40°$ observed in XRD patterns indicates the amorphous nature of our ZrO_2 materials. The TEM picture of a typical sample shows a quite porous system with regular organization of channels as observed in the case of mesoporous silicas (Fig. 2B).

The present study reveals that zirconia molecular sieves can be obtained via an electrostatic assembly. The optimization of the synthesis conditions leads to the formation of well-organized mesoporous zirconia. The recovered molecular sieves exhibit specific surface area up to 300 m^2/g and a uniform pore diameter. Different steps have been evidenced to describe the evolution of the materials formed in autoclave. In a first step the material is supermicroporous, then a breakdown of the wall leads to the formation of the mesoporous molecular sieves [13].

Titanium dioxide and iron oxides and oxyhydroxides are of technological importance as (photo)catalytic materials, sorbents, pigments, flocculents, coating, gas sensors and ion exchangers. In our laboratory, hollow microspheres of mesoporous titania with a thin shell of anatase structure have been prepared by using poly(ethylene oxide) assisted nanoparticle assembly in non-aqueous system. A high surface area of 378 m^2/g

and pore volume of 0.34 cm^3/g was obtained in the as-prepared sample with pore size of 2.6 nm [19]. A new mesoporous form of crystalline β-FeOOH (akaganeite) was also successfully prepared. The synthesized mesoporous β-FeOOH has a high surface area of 228 m^2/g and a pore size of 4.3 nm with a hierarchical scaffold-like structure formed through the aggregation and intergrowth of akaganeite nanorods [24].

4. Hierarchically structured meso–macroporous compositions

4.1. Pure metal oxides

4.1.1. Zirconium oxides

We demonstrated here a simple procedure for the synthesis of uniform mesoporous–macroporous metal oxide materials in the presence of one single surfactant of either cationic CTAB or non-ionic Brij 56 [66,67], without needing any secondary templating agents or any cosurfactants such as alcohol. Metal alkoxides were used as the inorganic precursors. The synthesized zirconia particles are monolithic with the particle size of 10 μm, exhibiting uniform macropores of 300–600 nm in diameter, revealed by both SEM and TEM micrographs (Fig. 5). The macrochannels are arranged parallel to each other and perpendicular to the tangent of the surface of the particle; the pores are funnel-like (tapered towards the center) in shape. The macroporous framework is composed of accessible mesochannels (~1.8 nm in diameter) with a wormhole-like array. The surface area could be high up to 700 m^2/g.

Using the mixture of zirconium propoxide and chloroform as the precursor can result in the production of an alternative structure of hierarchical microtubular nanoporous zirconia [68]. The synthesized particles are in a form of well-aligned hollow tubules with inner diameters of 0.5–1.5 μm and lengths ranging from 5 to 30 μm (Fig. 6). From the view of the profiles of the particles, it can be seen that the tubes are highly ordered and uniaxially arrayed into bundles but with open tips. Single tubules with a shorter length can also be seen in the samples. The tubular walls are composed of nanoparticles with accessible mesopores of a disordered wormhole-like array. The surface area and pore vol-

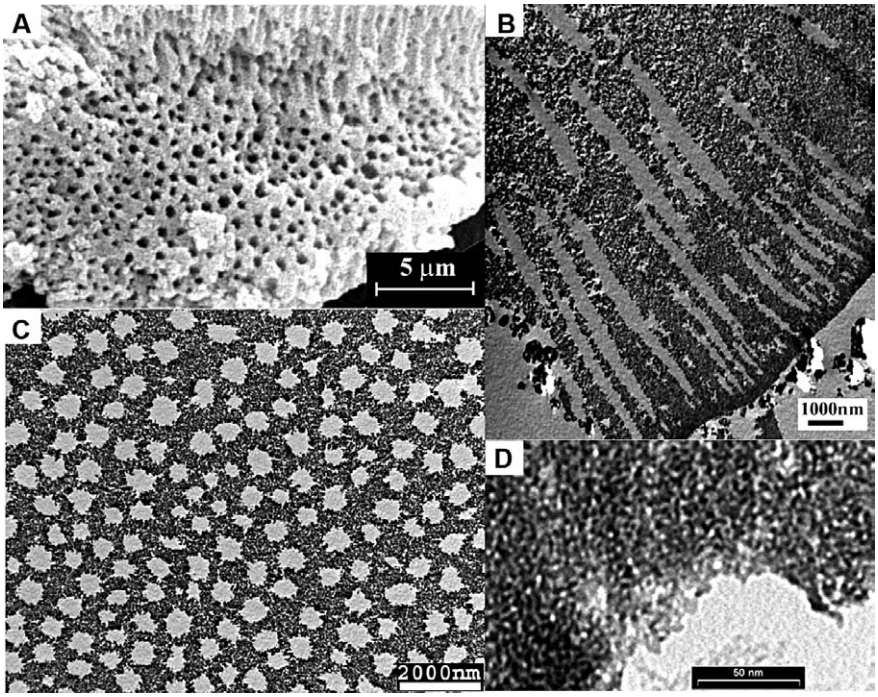

Fig. 5. Representative SEM image (**A**) of the synthesized meso–macroporous zirconia, showing the uniform macroporous structure; (**B**, **C**) are the cross-sectional TEM image of the macropores viewed parallel and perpendicular to the pores, respectively: (**D**) is the high-magnification TEM image of the macropore walls showing the wormhole-like mesostructure.

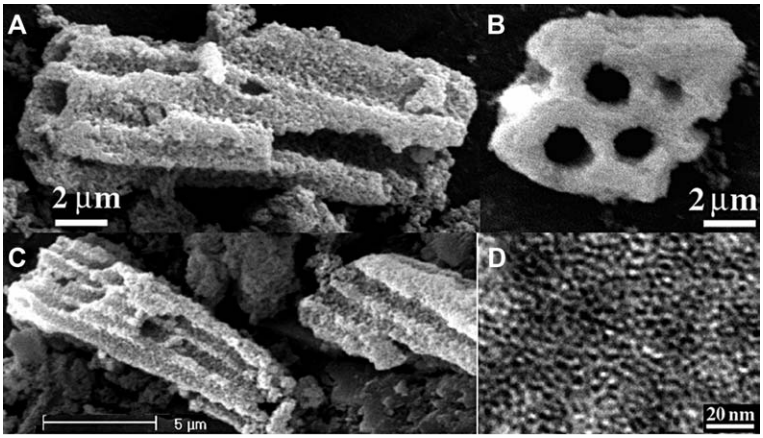

Fig. 6. Typical scanning electron microscopic images (**A**–**C**) of the resultant microtubular zirconias; (**B**) is the image viewed along the direction of tubules; (**D**) is a TEM image of the tubular walls showing wormhole-like mesostructure.

ume of the synthesized zirconia are extremely high up to 1100 m^2/g and 3.0 cm^3/g, respectively. The featured morphology formation, induced by the participation of chloroform in the synthesis, should be compatible with the significant increase of the surface areas and porosity of the resultant zirconias.

A new nanostructured ZrO_2 with the hierarchically three-length-scaled pore system was also synthesized [69]. The synthesized zirconia particles are also 10 μm in size with a regular array of macropores similar to Fig. 5A. The diameters of the macropores range from 300 to 500 nm which are uniformly distributed in the particles. A careful observation shows that the macroporous walls are composed of nanoparticles of about 25 nm in size, and the irregular small voids ranging between 20 and 60 nm which are the interparticle spaces resulted from the aggregation of these nanoparticles. These mesovoids are randomly distributed in the macroporous walls. High-magnification TEM images also reveal that these nanoparticles are mesostructured with a disordered wormhole-like assembly of accessible meso/micropores. A very high surface area of 903 m^2/g is obtained with the total pore volume of 1.01 cm^3/g. The adsorption isotherm exhibits the presence of supermicropores with the pore size at around 1.5 nm. Meanwhile, at the relative pressure higher than 0.85, a strong increase in nitrogen adsorbed volume is observed, evident of the large interparticular mesoporosity. This secondary porosity could be attributed to the mesovoids observed in the macroporous walls.

These very important progresses in the synthesis of hierarchical bimodal meso–macroporous and trimodal micro–meso–macroporous zirconias still reveal a crucial question from fundamental point of view as to what is the real role of surfactant molecules in the generation of the hierarchical structures although different scenarios concerning the function of surfactant molecules were developed [9,30]. The answer could be vital and our curiosity leads us to go further in the development of the simple, low-cost synthesis and modern strategy for the generation of the hierarchical porosities integrated in one body. The same synthesis was performed without surfactant molecules. Interestingly, the same hierarchy with bimodal meso–macroporosity similar to those obtained in the presence of surfactant molecules (Fig. 5) was observed. The real role of the surfactant molecules thus becomes fascinating [69–71]. We will discuss in detail in following section.

4.1.2. Titanium oxides

The synthetic media seem to be critical for the formation of hierarchically meso–macroporous structures of titania. Under aqueous solution system, a meso–macroporous structure similar to that of zirconia could be obtained but with larger macropore size (up to about 5 μm) and wormhole-like mesopores of 5 nm diameters. Under ethanol solution, an alternative macroporous structure was formed [72]. As shown in Fig. 7, the macroporous structure is hidden in the interiors of the titania particles. The particles have a quite thick shell, and their core possesses a sponge-like macroporous structure. The macropores are bicontinuous, three-dimensional, and interconnected with a uniform pore size gradient. Both the shell layers and the

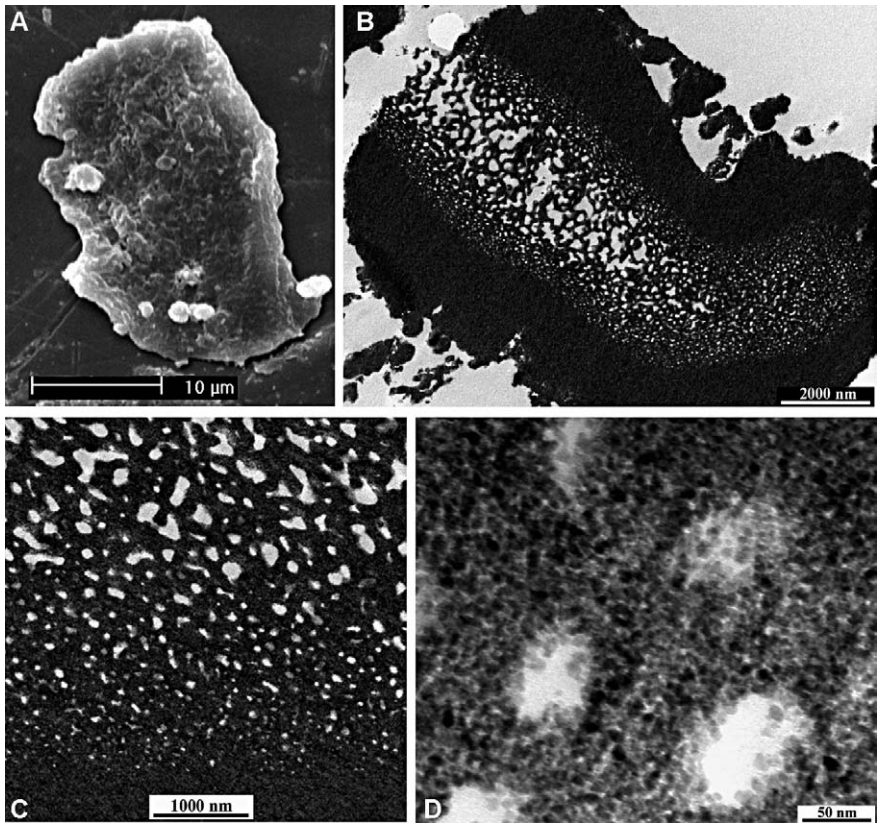

Fig. 7. SEM image (**A**), low-magnification TEM image (**B**) of an ultrathin section of CMI-Ti-80, (**C**) local enlarged image of (**B**), (**D**) high-magnification TEM image of (**B**).

macroporous framework of the core have a disordered wormhole-like mesoporous structure, formed by the agglomeration of TiO_2 nanoparticles. These accessible mesopores are connected randomly among the small TiO_2 particles and lack discernible long-range order in the pore arrangement, but interconnect with bicontinuous, three-dimensional macropores. It is expected that this kind of 'melon-like' interconnected meso–macroporous structure should be significant in its multiple applications including catalysis.

Fig. 8 shows the N_2 adsorption–desorption isotherms of the materials synthesized at 40 (CMI-Ti-40), 60 (CMI-Ti-60) and 80 °C (CMI-Ti-80). It is worth to indicate that with increasing the synthesis temperature, the porous wall varies from supermicroporous to well-defined mesoporous.

4.1.3. Aluminum oxides

The same type of meso–macroporous structure based on aluminum oxides was synthesized. The synthesized meso–macroporous aluminum oxides were crystalline with the structural type of AlOOH (boehmite) with the macropore sizes of 0.8–2 μm [73]. After calcination at 500 °C, AlOOH was converted to γ-Al_2O_3 with uniform meso–macrostructure. The TEM images of the boehmite and γ-Al_2O_3 specimens revealed that their

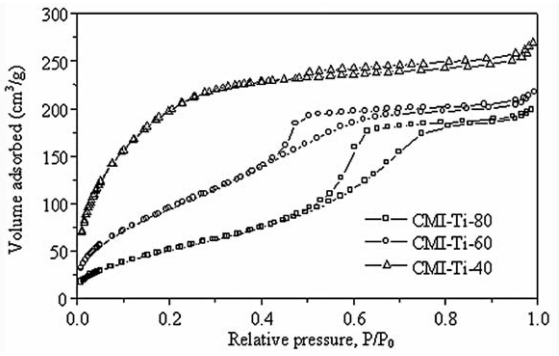

Fig. 8. N_2 adsorption–desorption isotherms of the synthesized titanias synthesized at 40, 60 and 80 °C.

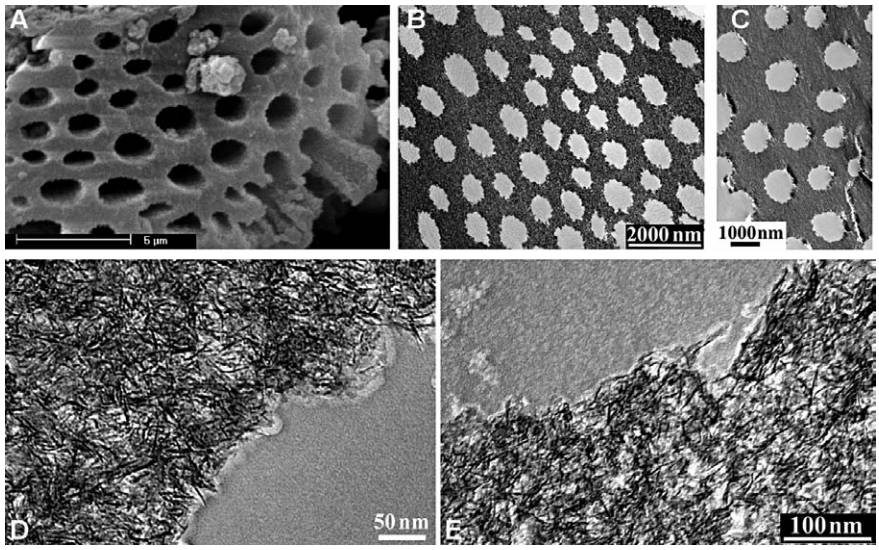

Fig. 9. SEM image (**A**) of synthesized boehmite AlOOH; cross-sectional TEM image of (**B**) boehimite; (**C**) cross-sectional TEM image of calcined γ-alumina; (**D**) and (**E**) are high-magnification TEM images of a macroporous region of (**B**) and (**C**), respectively, showing mesostructures of fiber-like nanoparticle assembly.

macroporous frameworks were composed of fibrous nanoparticles of boehmite and γ-Al_2O_3 with a scaffold-like array of hierarchical ordering, respectively (Fig. 9). The mesostructures of boehmite and γ-Al_2O_3 were formed through the scaffold-like aggregation and intergrowth of the boehmite and γ-Al_2O_3 nanofibers. The BET surface areas of AlOOH and γ-Al_2O_3 were 381 and 424 m^2/g, respectively. Solid-state ^{27}Al MAS NMR spectrum of the meso–macroporous AlOOH (boehmite) presents only one single signal of six-coordinate Al species, and the spectrum of the γ-Al_2O_3 shows the presence of four- and six-coordinate Al.

4.2. Binary metal oxide composites

By using the mixed alkoxide solutions, a series of binary oxide composite materials, including titania–zirconia, titania–alumina, alumina–zirconia, zirconia–silica and alumina–silica, with a hierarchically bimodal meso–macroporous structure similar to those of single metal oxides (Fig. 5) can be prepared [74]. In comparison with the meso–macrostructured single metal oxides, the introduction of secondary oxide leads to the significant improvement of the structural and textural properties of the resultant materials. The synthesized binary mixed oxides have a homogeneous distribution of the components and have higher surface areas than the single metal oxides. Moreover, not only the mesopore sizes, but also the macropore sizes of binary metal oxides could be tailored and controlled by the variation of the molar ratios of the metal precursors. The thermal stability of the binary oxide compositions could also be enhanced significantly. These meso-macrostructured binary oxide compositions should be significant for the use as advanced functional materials, especially in the catalysis applications.

4.3. Aluminosilicates

Aluminosilicate porous materials are a widely used composition in catalytic applications. The hierarchical structure of our aluminosilicate materials can be directly visualized by scanning electron microscopy (SEM) (Fig. 10). The morphologies of the particles of several tens to hundreds micrometers in size, show an array of regular and non-interconnected macrochannels with openings ranging from 0.5 to 2.0 μm (Fig. 10B). In comparison with the funnel-like channels of meso–macroporous zirconias, titanias and alumnias, the macropores of aluminosilicates are formed of more or less straight tubes, which are quite well parallel each other and perpendicular to the monolithic particle's surface. The regularity in size of the macrochannels is also clearly demonstrated from the TEM pictures (Fig. 10C). The TEM images show a disordered wormhole-like mesostructure of the walls separating the straight mac-

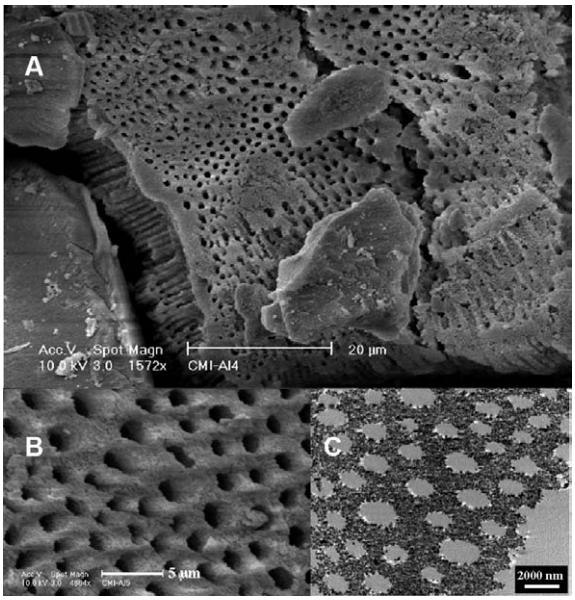

Fig. 10. SEM images (**A**–**B**) of the macro–mesoporous aluminosilicate material; (**C**): TEM image showing the cross-section of the macro-channels parallel to each other.

rochannels. The XRD pattern exhibits a single broad reflection in the zone of 20–35° (2θ) indicating the amorphous nature of our samples. Solid-state ^{27}Al-NMR measurements confirm the presence of Al atoms within the SiO_2 network. An intense peak located at 54 ppm can be attributed to tetrahedral, i.e. framework aluminum atoms. A weaker and somewhat broader peak at around 0 ppm indicates the presence of small part of the octahedral extra-framework Al.

The nitrogen adsorption–desorption isotherm is of type IV. The PSD is relatively broad, which is consistent with the absence of any regular structure seen in the XRD pattern. The maximum of the PSD is centered at about 3.9 nm. The specific surface areas of ethanol extracted and then calcined materials are very high, about 600 m^2/g.

Very recently, Collins et al. [75] reported an ammonia induced template-free and non-stirring method for the preparation of macroporous titania. They claimed that the rapid dropwise injection of the inorganic source into aqueous NH_3, the rates of hydrolysis/condensation and the nature of the alcohol by-product are important factors for the spontaneous formation of these materials. This observation confirms at least partly our reflections on the role of surfactant molecules in the creation of the hierarchy integrated in one body. The same synthesis of aluminosilicates was also performed without surfactant molecules and without ammonia as inductor. The similar non-interconnected tubular macrochannels are also observed and are parallel to each other and perpendicular to the monolithic (larger than 50 µm) particle's surface as observed in the case with surfactant molecules (Fig. 10). However, ^{27}Al MAS NMR spectrum showed that the octahedral aluminum atoms are in relative majority while tetrahedral Al are mainly observed in the presence of surfactant molecules. The poorly defined isotherm between types IV and II was obtained. This suggests that surfactant molecules help not only the incorporation of Al atoms into the framework but also the creation of mesopores to get real aluminosilicate compounds and the role of the surfactant molecules in the generation of the porous hierarchy integrated into one body still remains to be clarified while it could be not indispensable in the creation of the macropores [69–71].

4.4. Aluminophosphates and silicoaluminophosphates

The first synthesis of microporous crystalline zeolite-like aluminophosphate (AlPO) materials was performed by using organic agents (e.g. amines) as 'templates', which announced the beginning of the new era of zeolite and material sciences due to their unique physicochemical properties of potential application in fields such as catalysis or molecular sieving [76]. Substitution of Si in the framework of aluminophosphates imparts acidity to the resultant silicoaluminophosphate (SAPO) material and makes it active for a variety of acid-catalyzed reactions. The utilization of supramolecular assemblies of the surfactants as the structure-directing agents has recently been applied to the synthesis of mesostructured aluminophosphate-based materials [77], and some thermally stable mesoporous AlPOs and SAPOs were reported [78]. Large-pore (up to 12 nm) mesoporous AlPOs were synthesized by using triblock copolymer as a structure-directing agent [79].

The preparation of the hierarchically meso–macroporous AlPOs and SAPOs was realized without surfactant molecules in our laboratory. SEM studies of the products revealed the uniform macroporous structure in the AlPOs and SAPOs (Fig. 11A, B) [75]. The sizes of macropores are in the range of 300–1500 nm.

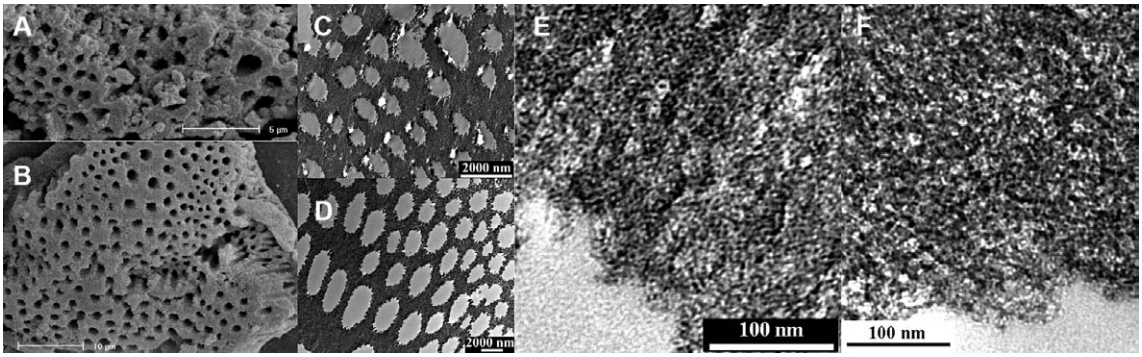

Fig. 11. SEM images of the autoclaved products of (**A**) AlPO and (**B**) SAPO. (**C**) and (**D**) are the cross-sectional TEM images of (**A**) and (**B**), respectively; (**E**) and (**F**) are the high-magnification images of the macroporous regions of (**C**) and (**D**), respectively.

Local regular array of the macropores can be seen in the both AlPO and SAPO particles. The macrochannels are mainly of one-dimensional orientation, parallel to each other, perforative through almost the whole particle. TEM images of the microtomed specimens further confirm the uniform and well-organized macroporous structures (Fig. 11C, D). High-magnification TEM images (Fig. 11E, F) of the cross-sectional AlPO and SAPO specimens demonstrated that their macroporous frameworks are composed of accessible mesopores with a disordered wormhole-like array. XRD patterns of the products indicate that the wall structures are amorphous.

N_2 adsorption–desorption isotherms are of classical type IV with a hysteresis loop of type H2, indicative of mesoporosity of good pore connectivity. A narrow PSD, suggestive of good homogeneity of these materials, is obtained. The mesopore sizes are in the range of 2.8–5.0 nm. The surface areas and pore volumes of AlPOs or SAPOs are quite high (270–459 m^2/g) compared to those of reported block copolymer-templated large-pore mesoporous AlPOs (115–261 m^2/g) [79]. The local structure and environments in these samples were investigated by the solid-state ^{27}Al and ^{31}P MAS NMR technique and clearly confirmed the formation of real AlPOs and SAPOs frameworks.

The synthesis of aluminosilicates, aluminophosphates and silicoaluminophosphates demonstrated the spontaneous formation of hierarchical mesoporous–macroporous materials with uniform macropore array and narrow mesopore size distribution in the absence of surfactants and templates. Using the synthesis of aluminophosphates as an example, the hydrolysis of Al-alkoxide precursors in the phosphate solution would result in the formation of aluminophosphate nanometer-sized particles. A network of narrow mesoporous channels could be generated in the aggregation of these regularly sized nanoparticles. A lot of butanol molecules were quickly released by the reaction of aluminum *sec*-butoxide and phosphatic ions and the polycondensation, which might produce microphase-separated domains of AlPO-based nanoparticles and water/alcohol channels [69–71,75]. Thus, a hierarchical structure of uniform macrochannels with mesoporous walls of nanoparticle assembly would form during the synergistic packing of the nanoparticles.

5. Conclusions

This review is not exhaustive and rather endeavors to illustrate the evolution occurred in our laboratory from highly ordered mesoporous silicas and metal oxides to more sophisticated hierarchically meso–macroporous compounds with various compositions. We extend also the synthesis of mesoporous silicas to their application in different fields such as the immobilization of highly efficient biomolecules in the mesochannels of our materials for the conception of new drug with delayed release effect and of nanobiosensors for metal ions dosing. The mesoporous silicas have been also used in our laboratory as matrix to prepare the nanosized ZnO in the mesochannels due to the interesting optical transparency of our materials. While the hierarchical materials with different pore sizes integrated in one body can be expected to combine reduced resistance to diffusion and high surface areas for yielding improved overall reaction and adsorption/separation

performances and can be extended to biological applications.

References

[1] M. Fröba, N. Oberender, Chem. Commun. (1997) 1729.
[2] M.J. MacLachlan, N. Coombs, G.A. Ozin, Nature 397 (1999) 681.
[3] Q. Huo, D.I. Margolese, U. Ciesla, P. Feng, T.E. Gier, P. Sieger, R. Leon, P.M. Petroff, F. Schüth, G.D. Stucky, Nature 368 (1994) 317.
[4] D.M. Antonelli, J.Y. Ying, Angew. Chem., Int. Ed. Engl. 35 (1996) 426.
[5] S.A. Bagshaw, T.J. Pinnavaia, Angew Chem., Int. Ed. Engl. 35 (1996) 1102.
[6] Z.R. Tian, W. Tong, J.Y. Wang, N.G. Duan, V.V. Krishnan, L.S. Suib, Science 276 (1997) 926.
[7] U. Ciesla, S. Schacht, G.D. Stucky, K.K. Unger, F. Schüth, Angew, Chem., Int. Ed. Engl. 35 (1996) 541.
[8] P. Yang, D. Zhao, D.I. Margolese, B.F. Chmelka, G.D. Stucky, Nature 396 (1998) 152.
[9] X. He, D. Antonelli, Angew. Chem., Int. Ed. Engl. 41 (2002) 214.
[10] J.L. Blin, A. Léonard, B.L. Su, Chem. Mater. 13 (2001) 3542.
[11] A. Léonard, J.L. Blin, M. Robert, P.A. Jacobs, A.K. Cheetham, B.L. Su, Langmuir 19 (2003) 5484.
[12] Q. Dai, L.Y. Shi, Y.G. Luo, J.L. Blin, D.J. Li, C.W. Yuan, B.L. Su, J. Photochem. Photobiol. A: Chem. 148 (2002) 295–301.
[13] J.L. Blin, R. Flamant, B.L. Su, Int. J. Inorg. Mater. 3 (2001) 959–972.
[14] J.L. Blin, C. Otjacques, G. Herrier, B.L. Su, Int. J. Inorg. Mater. 3 (2001) 75–86.
[15] J.L. Blin, A. Léonard, B.L. Su, J. Phys. Chem. B 105 (2001) 6070.
[16] G. Herrier, J.L. Blin, B.L. Su, Langmuir 17 (2001) 4422.
[17] G. Herrier, B.L. Su, Stud. Surf. Sci. Catal. 135 (2001) 1305–1313.
[18] A. Léonard, J.-L. Blin, G. Herrier, B.L. Su, Stud. Surf. Sci. Catal. 146 (2003) 243.
[19] T.Z. Ren, Z.Y. Yuan, B.L. Su, Chem. Phys. Lett. 374 (2003) 170–175.
[20] J.L. Blin, A. Becue, B. Pauwels, G. Van Tendeloo, B.L. Su, Micropor. Mesopor. Mater. 44 (45) (2001) 41–51.
[21] A. Leonard, J.-L. Blin, P.A. Jacobs, P. Grange, B.L. Su, Micropor. Mesopor. Mater. 63 (2003) 59–73.
[22] J.L. Blin, C. Otjacques, G. Herrier, B.L. Su, Langmuir 16 (2000) 4229–4236.
[23] J.L. Blin, B.L. Su, Langmuir 18 (2002) 5303–5308.
[24] Z.Y. Yuan, B.L. Su, Chem. Phys. Lett. 381 (2003) 710–714.
[25] C.F. Blanford, H. Yan, R.C. Schroden, M. Al-Daous, A. Stein, Adv. Mater. 13 (2001) 401.
[26] B.T. Holland, C.F. Blanford, A. Stein, Science 281 (1998) 538.
[27] D.M. Antonelli, Micropor. Mesopor. Mater. 33 (1999) 209.
[28] M. Antonietti, B. Berton, C. Göltner, H. Hentze, Adv. Mater. 10 (1998) 154.
[29] D. Zhao, P. Yang, B.F. Chmelka, G.D. Stucky, Chem. Mater. 11 (1999) 1174.
[30] A. Caruso, M. Antonietti, Adv. Funct. Mater. 12 (2002) 307.
[31] G.S. Attard, J.C. Glyde, C.G. Göltner, Nature 378 (1995) 366.
[32] S.A. Bagshaw, E. Prouzet, T.J. Pinnavaia, Science 269 (1995) 1242.
[33] P.T. Tanev, T.J. Pinnavaia, Science 267 (1995) 865.
[34] B. Lebeau, C.E. Fowler, S. Mann, C. Farcet, B. Charleux, C. Sanchez, J. Mater. Chem. 10 (2000) 2103.
[35] E. Prouzet, T.J. Pinnavaia, Angew. Chem., Int. Ed. Engl. 36 (1997) 516.
[36] E. Prouzet, F. Cot, G. Nabias, A. Larbot, P. Kooyman, T.J. Pinnavaia, Chem. Mater. 11 (1999) 1498.
[37] L. Sierra, J.L. Guth, Micropor. Mesopor. Mater. 27 (1999) 243.
[38] C. Boissière, A. Larbot, E. Prouzet, Chem. Mater. 2000 12 (1937).
[39] N.R.B. Coleman, G.S. Attard, Micropor. Mesopor. Mater. 44 (45) (2001) 73.
[40] D. Zhao, Q. Huo, J. Feng, B.F. Chmelka, G.D. Stucky, J. Am. Chem. Soc. 120 (1998) 6024.
[41] C.T. Kresge, M.E. Leonowicz, W.J. Roth, J.C. Vartuli, J.S. Beck, Nature 359 (1999) 710.
[42] J.S. Beck, J.C. Vartuli, W.J. Roth, M.E. Leonowicz, C.T. Kresge, K.D. Schmitt, C.T.W. Chu, D.H. Olson, E.W. Sheppard, S.B. McCuller, J.B. Higgins, J.L. Schlender, J. Am. Chem. Soc. 114 (1992) 10834.
[43] D.J. Mitchell, G.J.T. Tiddy, L. Waring, T. Bostock, M.P. McDonald, J. Chem. Soc. Faraday Trans. 79 (1983) 975 I.
[44] J. Patarin, B. Lebeau, R. Zana, Curr. Opin. Colloid. Interf. Sci. 7 (2002) 107.
[45] H.B.S. Chan, P.M. Budd, T. De V. Naylor, J. Mater. Chem. 11 (2001) 951.
[46] C. Boissière, A. Van der Lee, A. El Mansouri, A. Larbot, E. Prouzet, Chem. Commun. (1999) 2047.
[47] C. Boissière, A. Larbot, E. Prouzet, Stud. Surf. Sci. Catal. 129 (2000) 31.
[48] A. Davidson, Curr. Opin. Coll. Interf. Sci. 7 (2002) 92.
[49] M. Trau, N. Yao, E. Kim, Y. Xia, G.M. Whitesides, I.A. Aksay, Nature 390 (1997) 674.
[50] C.J. Brinker, J. Non-Cryst. Solids 100 (1988) 31.
[51] S. Kim, W. Zhang, T.J. Pinnavaia, Science 282 (1998) 2244.
[52] P.T. Tanev, T.J. Pinnavaia, Science 271 (1996) 1267.
[53] H. Yang, N. Coombs, G.A. Ozin, Nature 386 (1997) 692.
[54] G. Schultz-Ekloff, J. Rathousky, A. Zukal, Int. J. Inorg. Mater. 1 (1999) 97.
[55] M. Grün, I. Lauer, K.K. Unger, Adv. Mater. 9 (1997) 254.
[56] S. Schacht, Q. Huo, I.G. Voigt-Martin, G.D. Stucky, F. Schüth, Science 276 (1996) 768.
[57] Q. Huo, D. Zhao, J. Feng, K. Weston, S.K. Buratto, G.D. Stucky, Adv. Mater. 9 (1997) 974.
[58] G.A. Ozin, G.A.H. Yang, I. Sokolov, N. Coombs, Adv. Mater. 9 (1997) 662.

[59] W. Zhang, B. Glomski, T.R. Pauly, T.J. Pinnavaia, Chem. Commun. 1999 (1803).
[60] M. Shibagaki, K. Tabakahashi, H. Matsushita, Bull. Chem. Soc. Jpn 61 (1988) 3283.
[61] T. Yokoyama, T. Setoyama, N. Fujita, M. Nakajima, T. Maki, Appl. Catal. A 4 (1992) 149.
[62] J.A. Knowles, M.J. Hudson, Chem. Commun. (1995) 2083.
[63] A. Kim, P. Bruinsma, Y. Chen, L.Q. Wang, J. Liu, Chem. Commun. (1997) 161.
[64] G. Pacheco, E. Zhao, A. Garcia, A. Sklyarov, J.J. Fripiat, Chem. Commun. (1997) 491.
[65] P. Yang, E. Zhao, D.I. Margolese, B.F. Chmelka, G.D. Stucky, Chem. Mater. 11 (1999) 2813.
[66] J.L. Blin, A. Léonard, Z.Y. Yuan, L. Gigot, A. Vantomme, A.K. Cheetham, et al., Angew. Chem., Int. Ed. Engl. 42 (2003) 2875.
[67] Z.Y. Yuan, A. Vantomme, A. Léonard, B.L. Su, Chem. Commun. (2003) 1558.
[68] T.Z. Ren, Z.Y. Yuan, B.L. Su, Chem. Phys. Lett. 388 (2004) 46.
[69] A. Vantomme, Z.Y. Yuan, B.L. Su, New J. Chem. 28 (2004) 1083.
[70] A. Leonard, B.L. Su, Chem. Commun. (2004) 1674.
[71] T.Z. Ren, Z.Y. Yuan, B.L. Su, Chem. Commun. (2004) 2730.
[72] Z.Y. Yuan, T.Z. Ren, B.L. Su, Adv. Mater. 151 (2003) 462.
[73] T.Z. Ren, Z.Y. Yuan, B.L. Su, Langmuir 20 (2004) 1531.
[74] Z.Y. Yuan, T.Z. Ren, A. Vantomme, B.L. Su, Chem. Mater. 16 (2004) 5096.
[75] A. Collins, D. Carriazo, S.A. Davis, S. Mann, Chem. Commun. (2004) 568.
[76] S.T. Wilson, B.M. Lok, C.A. Messina, T.R. Cannan, E.M. Flanigen, J. Am. Chem. Soc. 104 (1982) 1146.
[77] S. Oliver, A. Kuperman, N. Coombs, A. Lough, G.A. Ozin, Nature 378 (1995) 47.
[78] T. Kimura, Y. Sugahara, K. Kuroda, Chem. Commun. (1998) 559.
[79] L. Wang, B. Tian, J. Fan, X. Liu, H. Yang, C. Yu, et al., Micropor. Mesopor. Mater. 67 (2004) 123.